SUPPORTING INFORMATION

Site-selective Protonation of the One-electron Reduced Cofactor in [FeFe]-Hydrogenase

Konstantin Laun[a,b], Iuliia Baranova[a,c], Jifu Duan[d], Leonie Kertess[d], Florian Wittkamp[e], Ulf-Peter Apfel[e,f], Thomas Happe[d], Moritz Senger[a,g]*, Sven T. Stripp[a]*

* E-mail: moritz.senger@kemi.uu.se and sven.stripp@fu-berlin.de

Contents:

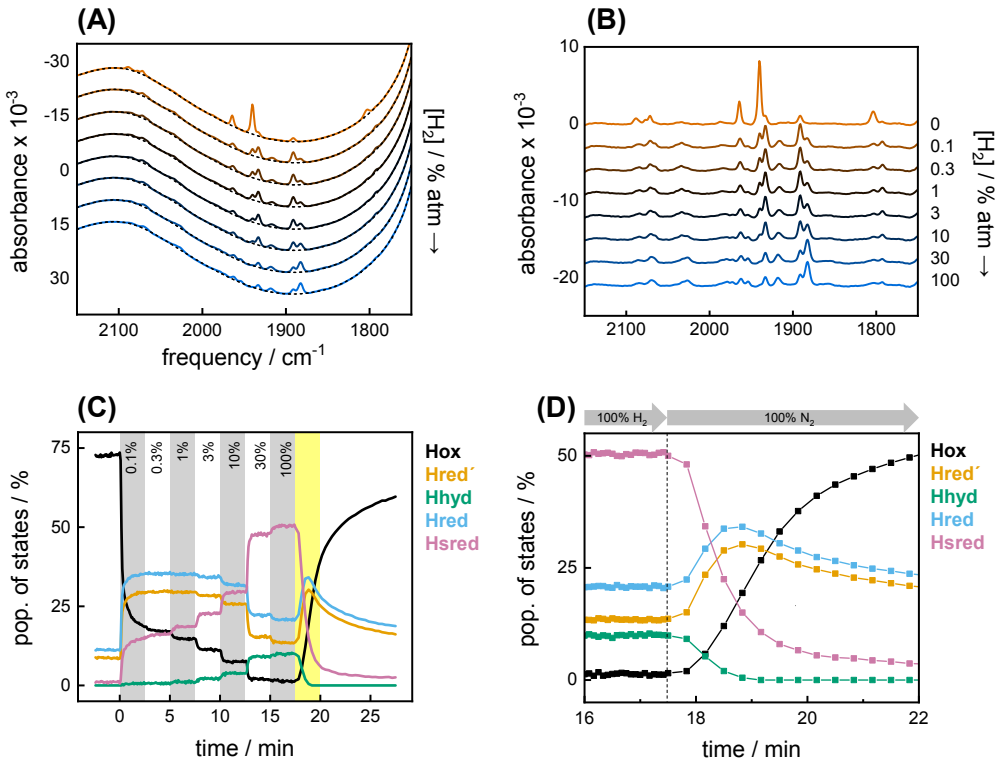

Figure S1 | Global fit analysis of ATR FTIR spectroscopy under gas control. An exemplary data set at pH 7 is shown resembling Figure 3 in the main script. No manual data manipulation was performed. Unprocessed **(A)** and background-corrected **(B)** ATR FTIR absorbance spectra between 0–100% H_2 in N_2 carrier gas (top to bottom), recorded after 2.5 min equilibration time for each step. Dashed lines represent the background as simulated by a low-frequency polynomial fit (physically representing the 'combination' band of liquid water). **(C)** ATR FTIR spectroscopy allows following the changes in H-cluster states in a dynamic fashion. Here, the sum area of 2 CN^- and 3–4 CO bands (see Figure S3) defines the 'population' of redox species in %, plotted against time. Higher concentrations of atmospheric H_2 induce an increasingly amount of reduced and 'super-reduced' H-cluster states. Note the fast equilibration of all H-cluster states within 1–3 minutes. **(D)** When the atmosphere over the protein film was changed from 100% H_2 back to 100% N_2 (t = 17.5 min, dashed line), **Hsred** and **Hhyd** convert into **Hox** (auto-oxidation) *via* a transient increase of **Hred** and **Hred´** (see Figure S6).

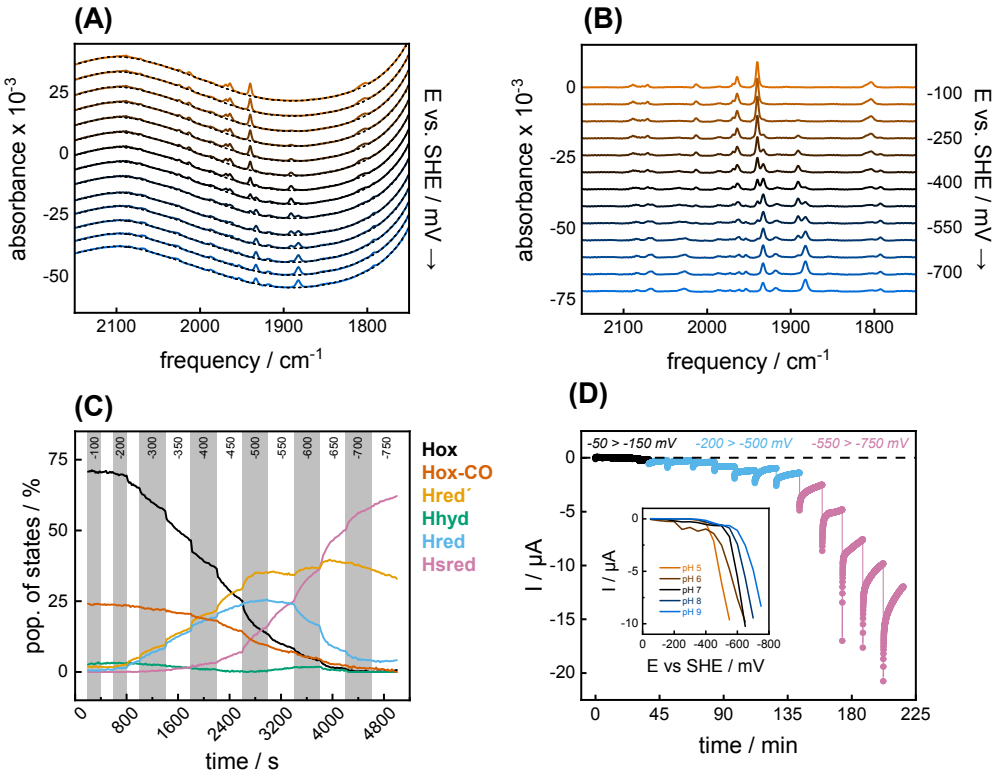

Figure S2 | Global fit analysis of ATR FTIR spectroscopy under potential control. An exemplary data set at pH 6 is shown resembling Figure 5 in the main script. No manual data manipulation was performed. Unprocessed **(A)** and background-corrected **(B)** ATR FTIR absorbance spectra from -100 to -750 mV vs SHE (top to bottom), recorded after 20 min equilibration time for each potential step. Dashed lines represent the background as simulated by a low-frequency polynomial fit (physically representing the 'combination' band of liquid water). **(C)** ATR FTIR spectroscopy allows following the changes in H-cluster states in a dynamic fashion. Here, the sum area of 2 CN^- and 3–4 CO bands (see Figure S3) defines the 'population' of redox species in %, plotted against time. Note the equilibration of most H-cluster states within 20 minutes. **(D)** Current vs. time and potential, recorded during a similar experiment as in panel C but at pH 5. At each potential step, the current 'jumps' and equilibrates after 20 min; however, no steady-state conditions are reached for E < -500 mV (presumably due to the onset of catalysis). Under oxidizing conditions **Hox** prevails (black traces), under mildly reducing conditions **Hred** and **Hred´** are dominant (light blue traces), and **Hsred** is accumulated at strongly reducing conditions (rose traces). Inset: for higher pH values, the onset of catalysis shifts to more negative potentials.

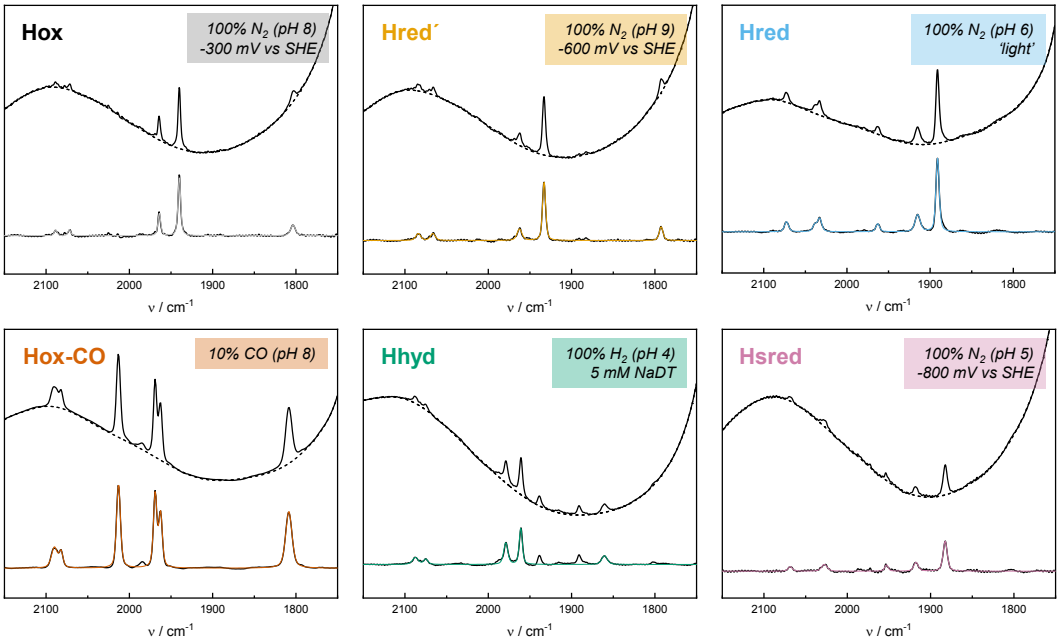

Figure S3 | FTIR reference spectra of key H-cluster states. In different experiments, pure H-cluster states were achieved. All panels depict unprocessed ATR FTIR spectra with the background contribution shown as a dashed line (simulated by a low-frequency polynomial fit that physically represents the 'combination' band of liquid water). Additionally, the background-corrected spectrum is plotted, overlayed with a Voigt profile (50% Gauss, 50% Lorentz distribution) of the respective H-cluster spectrum (2 CN^- and 3–4 CO bands). These fits comprise band frequency, band intensity, full width at half-max (FWHM), and the ratio of band areas (see Table S1). **Hox** was accumulated at pH 9, oxidizing potentials of -300 mV vs SHE, and N_2 purging as detailed in this work. **Hox-CO** was accumulated at pH 8 including 10% CO gas in the N_2 atmosphere.[1] **Hred´** was accumulated at pH 9, reducing potentials of -600 mV vs SHE, and N_2 purging as detailed in this work. **Hhyd** was accumulated at pH 5 and in the presence of 5 mM sodium dithionite under 100% H_2.[2] The spectrum includes a small contribution of other H-cluster states as indicated. **Hred** was accumulated upon irradiation (505 nm) in the presence of eosin Y and EDTA (100%N_2, pH 5).[3] **Hsred** was accumulated at pH 5, reducing potentials of -800 mV vs SHE, and N_2 purging as detailed in this work. We cannot exclude a minor population of the cryogenic **HsredH**$^+$ state in this spectrum.[4,5]

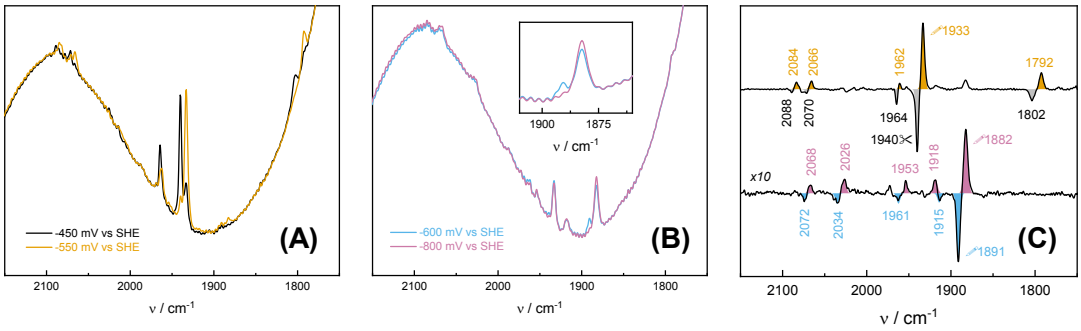

Figure S4 | Supporting difference spectra. Calculating the difference between spectra allows highlighting small changes in the IR signatures of H-cluster states. This procedure is experimentally demanding because any unspecific changes must be avoided. To this end, we exploited the pH dependance of Hred´ and Hred/Hsred to produce highly specific difference spectra. **(A)** 'Absolute' spectra of *Cr*HydA1 at -450 mV vs SHE (black) and -550 mV vs SHE (brown) at pH 9 that allow analyzing the **Hox⋋Hred´** transition. **(B)** 'Absolute' spectra of *Cr*HydA1 at -600 mV vs SHE (light blue) and -800 mV vs SHE (rose) at pH 5 that allow analyzing the **Hred⋋Hsred** transition. Note that the transition includes < 10% of the overall band intensity (inset). **(C)** Difference spectra based on data in panels A and B. More oxidized H-cluster state appear 'negative'. The overall downshift of the cofactor bands from **Hox⋋Hred´** (upper spectrum) and **Hred ⋋ Hsred** (bottom spectrum) has been attributed to a reduction of the [4Fe-4S] cluster.[6,7] Opposed to the **Hox⋋Hred´** difference spectrum, the **Hred⋋Hsred** difference spectrum shows no signal around 1800 cm^{-1}. This highlights the lack of a μCO ligand at the reduced diiron site. Moreover, note the absence of any other H-cluster species, which confirms the assignment of bands at 1961 cm^{-1} and 1953 cm^{-1} to **Hred** and **Hsred**, respectively. The small band at 1972 cm^{-1} is unrelated to any known redox state. It has been assigned to **Hhyd:red** under cryogenic conditions[4]; however, the spectrum lacks the μCO band at 1851 cm^{-1}.

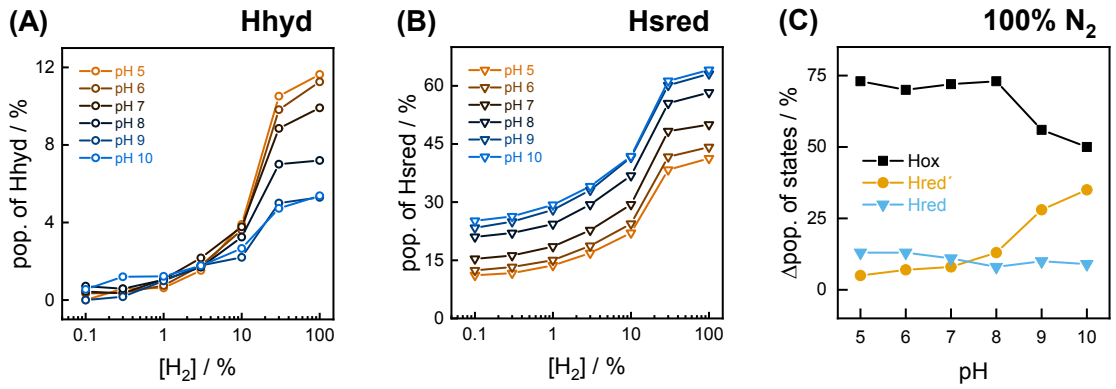

Figure S5 | Accumulation of H-cluster states as a function of [H_2] and pH. (A) Population of **Hhyd** between pH 10–5 at 0.1–100% H_2 under steady-state conditions. At elevated concentration of H_2, low pH values promote accumulation of **Hhyd**. This is in line with previous observations, although the sample did not include any sodium dithionite.[2] Apparently, the lack of chemical reductant can be partly compensated by H_2 at low pH values. **(B)** Population of **Hsred** between pH 10–5 at 0.1–100% H_2 under steady-state conditions. Different to **Hred**, **Hsred** was accumulated more prominently at alkaline pH values. This may indicate formation of **Hsred** from both **Hred** and **Hred´**, in particular under high pH conditions that suppress a concerted enrichment of **Hhyd**. **(C)** Population of **Hox**, **Hred´**, and **Hred** between pH 10–5 in the absence of H_2 (100% N_2). **Hox** clearly dominates but at alkaline pH values, auto-oxidation (see Figure S6) becomes increasingly slow. This gives rise to a higher population of **Hred´** as a 'quasi' resting state in as-isolated samples. The effect is notably less pronounced for **Hred**.

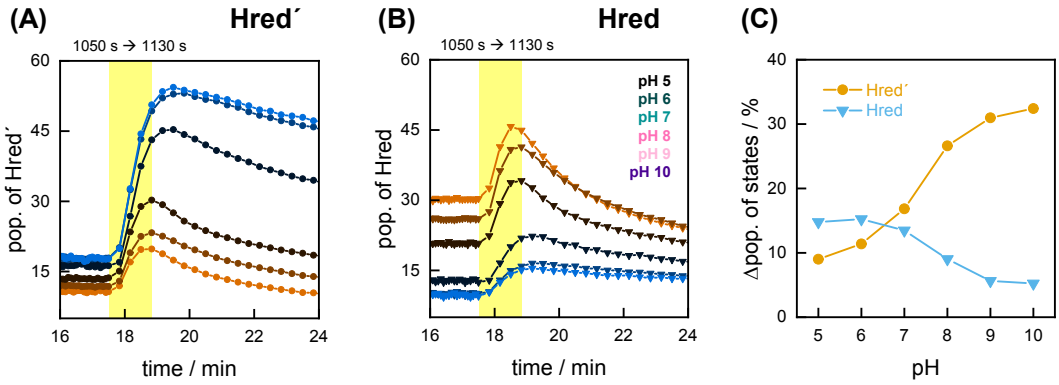

Figure S6 | pH dependence of auto-oxidation. Upon removal of H_2 from the gas phase, the $2e^-$-reduced states **Hsred** and **Hhyd** decay into **Hox** *via* a transient increase of **Hred´ (A)** and **Hred (B)**. This is a result of auto-oxidation (H_2 evolution activity of *C*rHydA1 in the absence of H_2) and intermolecular electron transfer between neighboring molecules in the protein film. **(C)** The difference in the population of **Hred´** and **Hred** at t = 1130 s *minus* t = 1050 s (yellow mark-up, eq. N_2 *minus* H_2) is plotted against pH. The graph illustrates that the diverging pH dependence observed under increasing concentrations of H_2 (Figure 5C in the main script) is well conserved in the process of auto-oxidation transfer as well.

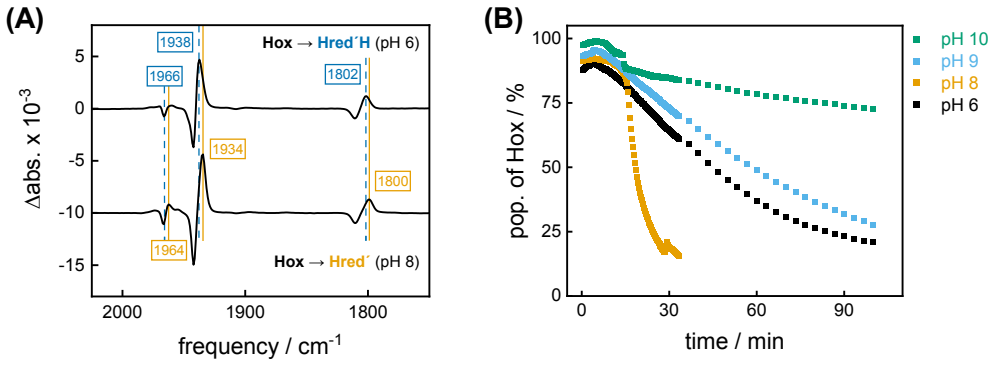

Figure S7 | pH dependence of the H_2 oxidation kinetics of cofactor variant PDT. Cofactor variant *Cr*HydA1^{pdt} was produced as previously described.[8] To probe the effect of sample pH on the H_2 oxidation kinetics of *Cr*HydA1^{pdt}, 1 mM protein solution was mixed 1:1 with 100 mM mixed buffer pH 10–6. Sample was dried and re-hydrated on the ATR crystal and purged with N_2 until the film consisted of ~100% **Hox** (60–90 min). Then, the N_2 gas stream was switched to 100% H_2 to followed the decrease of **Hox** and increase of **Hred´** or **Hred´H**. See ref. [9] for details on the latter state. **(A)** 'H_2 *minus* N_2' ATR FTIR difference spectrum at pH 6 and pH 8. Note the accumulation of **Hred´H** over **Hox** at pH 6 (upper spectrum) in variance to pH 8 where only **Hred´** was observed. **(B)** Decrease of **Hox** over time for different pH values. We observed an increase of H_2 oxidation activity from pH 10–8 while at pH 6, the kinetics are significantly diminished. The former observation is explained by an increasingly efficient protonation of the [4Fe-4S] cluster in the presence of the natural reductant H_2. This results in an increasingly faster accumulation of **Hred´** and agrees with PCET to the [4Fe-4S] cluster.[8–10] At pH 6, **Hred´** was barely observed and **Hox** is lost in favor of **Hred´H**; however, much slower than at pH 8. Previously, we could describe the **Hred´H** state with two protonation events at the [4Fe-4S] cluster[9], which would result in a lower pKa value compared to **Hred´**. The observed decrease of H_2 oxidation kinetics at pH 6 is in agreement with this model.

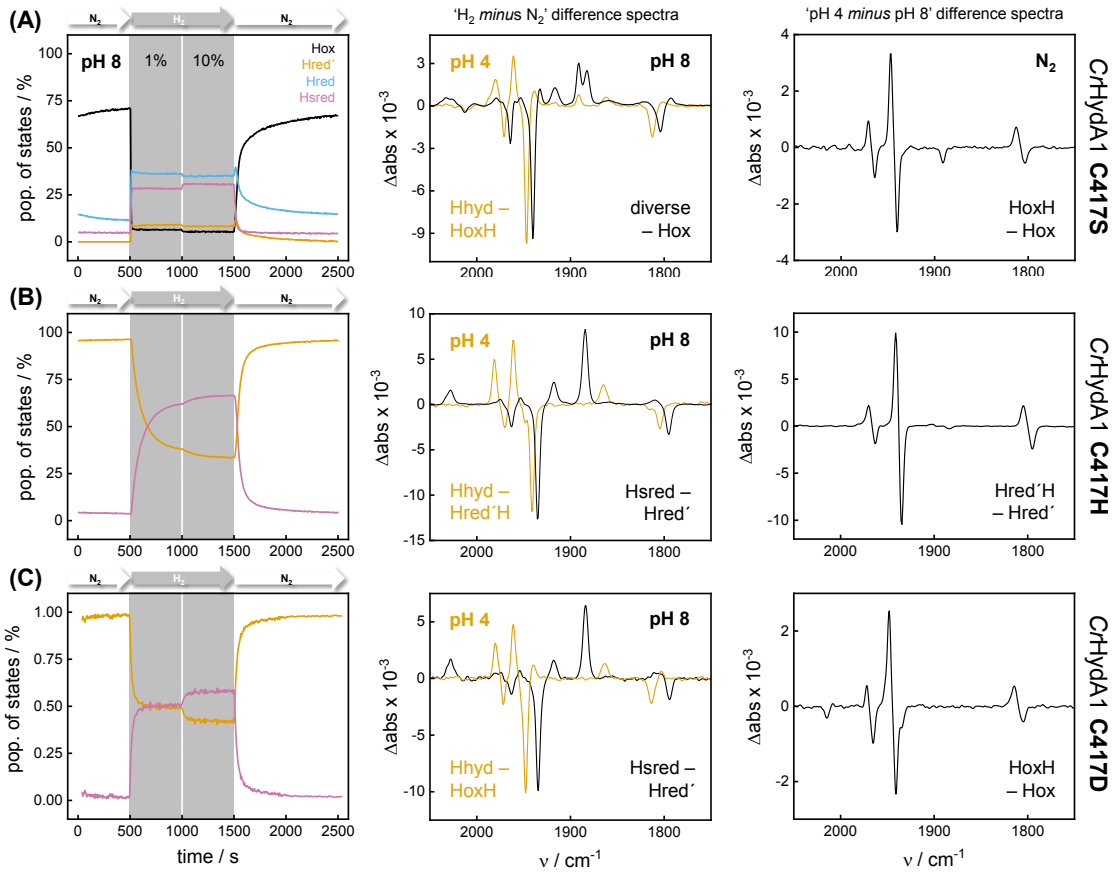

Figure S8 | Characterization of cysteine variants. We analyzed three variants of cysteine C417 at the [4Fe-4S] cluster under H_2 oxidation conditions and different pH values. The production of enzyme was reported previously.[11,12] Column 1 (C1, left side) depicts the composition of H-cluster states as a function of time and gas composition (pH 8). Column 2 (C2, middle) shows H_2 minus N_2 difference spectra at pH 8 (black traces) and pH 4 + 2 mM DT (brown traces). Column 3 (C3, right side) shows pH 4 minus pH 8 differences spectra recorded under 100% N_2.

(A) C417S. [C1] The composition of H-cluster states is comparable to native *Cr*HydA1, only the percentage of **Hred´** is lower (compare Figure 3 in the main script). Up to 10% H_2, we did not observe enrichment of **Hhyd**. [C2] No significant shifts were observed for the IR signature of **Hox**, **Hred´**, **Hred**, and **Hsred**. At pH 4 + 2 mM DT, **HoxH** converted into **Hhyd** in the presence of H_2. [C3] At pH 4 + 2 mM DT, **HoxH** converted into **Hhyd**.

(B) C417H. [C1] In the presence of N_2, the variant adopted **Hred´** as resting state and converted relatively slow into **Hsred** under H_2. [C2] The difference spectrum suggested conserved IR signatures as compared to native *Cr*HydA1. At pH 4 + 2 mM DT, **Hred´H** converted into **Hhyd** in the presence of H_2. [C3] Interestingly, **Hred´** converted into **Hred´H** at pH 4 + 2 mM DT, and neither **Hox** nor **HoxH** was observed.

(C) C417D. [C1] In the presence of N_2, the variant adopted **Hred´** as resting state and converted rapidly into **Hsred** under H_2. [C2] The difference spectrum suggested conserved IR signatures as compared to native *Cr*HydA1. At pH 4 + 2 mM DT, **HoxH** converted into **Hhyd** in the presence of H_2. [C3] At pH 4 + 2 mM DT, **HoxH** converted into **Hhyd**.

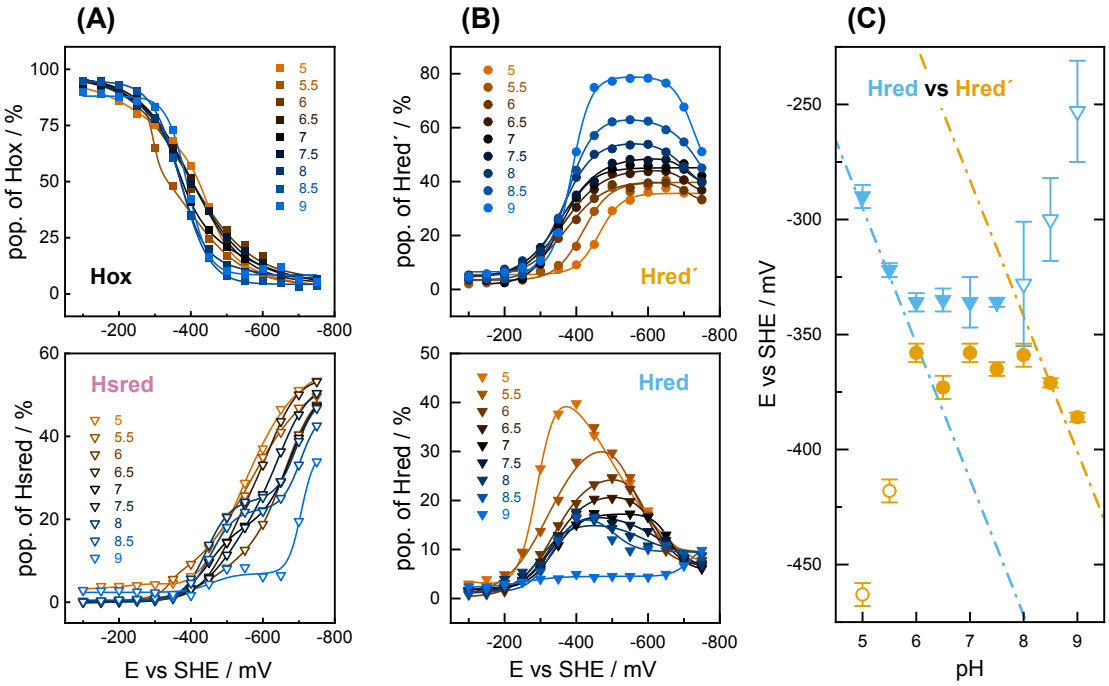

Figure S9 | Accumulation of H-cluster states as a function of potential and pH. The population of each state at the end of the incubation period (see Figure S2) is plotted against potential. Each trace is fitted with a bi-sigmoidal function to contribute for increase and/or decrease of multiple states (solid lines). A significant contribution of **Hhyd** to the spectra was not observed. **(A) Hox** reflects the sum of all trends observed for the reduced species. The mean midpoint potential is around -400 mV vs SHE. A trend for the accumulation of **Hsred** was observed for potential more negative than -650 mV vs SHE. Opposite to our H_2 oxidation experiments (Figure S5), a preferential enrichment of **Hsred** at low pH conditions was noted, in agreement with the trends observed for **Hred**. **(B)** The panels for **Hred´** and **Hred** show the same data sets as in the main script (compare Figure 6) but including the fitted traces here. **(C)** The bi-sigmoidal fits suggest midpoint potentials (E_M) for the transition **Hox→Hred´** (brown circles) and **Hox→Hred** (light blue triangles) that are plotted against pH in a Pourbaix diagram. The fit quality is depicted by the 'error bars', which allows excluding certain E_M values in the analysis (e.g., the absolute population of. **Hred** is too low to extract meaningful values between pH 9–8). We note a ~60 mV/pH decrease of E_M for **Hox→Hred´** in the alkaline region and a similar decrease of E_M for **Hox→Hred** in the acidic region (dashed-dotted lines). These trends are in agreement with site-selective protonation in the formation of both **Hred´** and **Hred**. The *increase* of E_Ms (open circles or triangles) hints at 'competition' between these two states. Around pH 7, no pronounced pH dependance is observed.

Table S1 – Global fit parameters.

	ligand	frequency	FWHM	ratio
Hox	μCO	1802	6	0.2
	tCO	1940	5	1
		1964.5	4	0.3
	tCN	2071.5	6	0.1
		2088.5	6	0.1
Hred´	μCO	1792	6	0.2
	tCO	1933	5	1
		1961.5	4	0.2
	tCN	2070	6	0.1
		2084	6	0.1
Hhyd	μCO	1860.5	7	0.25
	tCO	1960.5	4	1
		1979	6	0.6
	tCN	2075	6	0.1
		2088	6	0.15
Hred	tCO	1891	6	1
		1915	6	0.25
		1962	5	0.1
	tCN	2033	6	0.2
		2072.5	6	0.1
Hsred	tCO	1882.5	6	1
		1918	6	0.3
		1953.5	5	0.15
	tCN	2026.5	6	0.2
		2066.5	6	0.15
Hox-CO	μCO	1808	8	0.6
	tCO	1962	4	0.6
		1968	4	0.85
		2012	4	1
	tCN	2082	4	0.15
		2092	4	0.15

References

(1) Senger, M.; Mebs, S.; Duan, J.; Wittkamp, F.; Apfel, U.-P.; Heberle, J.; Haumann, M.; Stripp, S. T. Stepwise Isotope Editing of [FeFe]-Hydrogenases Exposes Cofactor Dynamics. *Proc. Natl. Acad. Sci. U. S. A.* **2016**, *113* (30), 8454–8459. https://doi.org/10.1073/pnas.1606178113.

(2) Winkler, M.; Senger, M.; Duan, J.; Esselborn, J.; Wittkamp, F.; Hofmann, E.; Apfel, U.-P.; Stripp, S. T.; Happe, T. Accumulating the Hydride State in the Catalytic Cycle of [FeFe]-Hydrogenases. *Nat. Commun.* **2017**, *8* (16115), 1–7. https://doi.org/10.1038/ncomms16115.

(3) Senger, M.; Eichmann, V.; Laun, K.; Duan, J.; Wittkamp, F.; Knör, G.; Apfel, U.-P.; Happe, T.; Winkler, M.; Heberle, J.; et al. How [FeFe]-Hydrogenase Facilitates Bidirectional Proton Transfer. *J. Am. Chem. Soc.* **2019**, *141* (43), 17394–17403. https://doi.org/10.1021/jacs.9b09225.

(4) Lorent, C.; Katz, S.; Duan, J.; Julia Kulka, C.; Caserta, G.; Teutloff, C.; Yadav, S.; Apfel, U.-P.; Winkler, M.; Happe, T.; et al. Shedding Light on Proton and Electron Dynamics in [FeFe] Hydrogenases. *J. Am. Chem. Soc.* **2020**, *142* (12), 5493–5497. https://doi.org/10.1021/jacs.9b13075.

(5) Birrell, J. A.; Pelmenschikov, V.; Mishra, N.; Wang, H.; Yoda, Y.; Rauchfuss, T. B.; Cramer, S. P.; Lubitz, W.; Debeer, S. Spectroscopic and Computational Evidence That [FeFe] Hydrogenases Operate Exclusively with CO-Bridged Intermediates. *J. Am. Chem. Soc.* **2020**, *142* (1), 222–232. https://doi.org/10.1021/jacs.9b09745.

(6) Adamska-Venkatesh, A.; Silakov, A.; Lambertz, C.; Rüdiger, O.; Happe, T.; Reijerse, E.; Lubitz, W. Identification and Characterization of the "Super-Reduced" State of the H-Cluster in [FeFe] Hydrogenase: A New Building Block for the Catalytic Cycle? *Angew. Chemie Int. Ed.* **2012**, *51* (46), 11458–11462. https://doi.org/10.1002/anie.201204800.

(7) Adamska-Venkatesh, A.; Krawietz, D.; Siebel, J. F.; Weber, K.; Happe, T.; Reijerse, E.; Lubitz, W. New Redox States Observed in [FeFe] Hydrogenases Reveal Redox Coupling within the H-Cluster. *J. Am. Chem. Soc.* **2014**, *136* (32), 11339–11346. https://doi.org/10.1021/ja503390c.

(8) Senger, M.; Laun, K.; Wittkamp, F.; Duan, J.; Haumann, M.; Happe, T.; Winkler, M.; Apfel, U.-P.; Stripp, S. T. Proton-Coupled Reduction of the Catalytic [4Fe-4S] Cluster in [FeFe]-Hydrogenases. *Angew. Chemie Int. Ed.* **2017**, *56* (52), 16503–16506. https://doi.org/10.1002/anie.201709910.

(9) Senger, M.; Mebs, S.; Duan, J.; Shulenina, O.; Laun, K.; Kertess, L.; Wittkamp, F.; Apfel, U.-P.; Happe, T.; Winkler, M.; et al. Protonation/Reduction Dynamics at the [4Fe–4S] Cluster of the Hydrogen-Forming Cofactor in [FeFe]-Hydrogenases. *Phys. Chem. Chem. Phys.* **2018**, *20* (5), 3128–3140. https://doi.org/10.1039/C7CP04757F.

(10) Laun, K.; Mebs, S.; Duan, J.; Wittkamp, F.; Apfel, U.-P.; Happe, T.; Winkler, M.; Haumann, M.; Stripp, S. T. Spectroscopical Investigations on the Redox Chemistry of [FeFe]-Hydrogenases in the Presence of Carbon Monoxide. *MOLECULES* **2018**, *23* (7), 1669. https://doi.org/10.3390/molecules23071669.

(11) Rodríguez-Maciá, P.; Kertess, L.; Burnik, J.; Birrell, J. A.; Hofmann, E.; Lubitz, W.; Happe, T.; Rüdiger, O. His-Ligation to the [4Fe-4S] Subcluster Tunes the Catalytic Bias of [FeFe] Hydrogenase. *J. Am. Chem. Soc.* **2019**, *141* (1), 472–481. https://doi.org/10.1021/jacs.8b11149.

(12) Kertess, L.; Adamska-Venkatesh, A.; Rodríguez-Maciá, P.; Rüdiger, O.; Lubitz, W.; Happe, T. Influence of the [4Fe-4S] Cluster Coordinating Cysteines on Active Site Maturation and Catalytic Properties of C. Reinhardtii [FeFe]-Hydrogenase. *Chem. Sci.* **2017**, *8* (12), 8127–8137. https://doi.org/10.1039/c7sc03444j.